nature biotechnology

Renal clearance of quantum dots

Hak Soo Choi[1], Wenhao Liu[2], Preeti Misra[1], Eiichi Tanaka[1], John P Zimmer[2], Binil Itty Ipe[2], Moungi G Bawendi[2] & John V Frangioni[1,3]

The field of nanotechnology holds great promise for the diagnosis and treatment of human disease. However, the size and charge of most nanoparticles preclude their efficient clearance from the body as intact nanoparticles. Without such clearance or their biodegradation into biologically benign components, toxicity is potentially amplified and radiological imaging is hindered. Using intravenously administered quantum dots in rodents as a model system, we have precisely defined the requirements for renal filtration and urinary excretion of inorganic, metal-containing nanoparticles. Zwitterionic or neutral organic coatings prevented adsorption of serum proteins, which otherwise increased hydrodynamic diameter by >15 nm and prevented renal excretion. A final hydrodynamic diameter <5.5 nm resulted in rapid and efficient urinary excretion and elimination of quantum dots from the body. This study provides a foundation for the design and development of biologically targeted nanoparticles for biomedical applications.

Although targeted nanoparticles hold promise for the detection and treatment of human disease, toxicity—either potential or real—remains the major roadblock to clinical translation[1]. Historically, the US Food and Drug Administration has required that agents injected into the human body, especially diagnostic agents, be cleared completely, in a reasonable amount of time. This policy makes sense in that total body clearance minimizes the area under the exposure curve. It also minimizes the chance that the agent will interfere with other diagnostic tests. For example, gold, used extensively in the nanotechnology literature, has an X-ray attenuation coefficient 150-fold higher than even bone and at doses injected intravenously would likely preclude accurate computed tomographic (CT) scanning, especially in organs such as the liver, where it eventually accumulates.

Against this backdrop is the inherent stability of most nanoparticles. Indeed, a recent study suggests that quantum dots with the appropriate organic coating are retained in the body for at least 2 years and remain fluorescent[2]. When considering that many nanometer-sized objects proposed for clinical use contain heavy metals, regulatory approval of such stable particles is unlikely, and the type of long-term toxicity studies that would be required for such approval will continue to discourage clinical translation.

A potential solution to this conundrum is to focus on the physiology underlying biodistribution and clearance of agents injected intravenously into the body. For globular proteins, a hydrodynamic diameter of ~5–6 nm is associated with the ability to be cleared rapidly from the body by renal filtration and urinary excretion (**Table 1**). Nanoparticle toxicity would be minimized, if not eliminated, if there were a way to clear the particles from the body. However, it is unknown what the renal filtration threshold is for metal-based nanometer-sized objects and which organic coatings are compatible with renal clearance. In this study, we use fluorescent quantum dots as a model system to define the hydrodynamic diameter and surface charge combination that permits rapid body elimination of nanometer-sized objects.

To define the renal filtration threshold, a precise size-series of extremely small quantum dots was synthesized. All quantum dots had a CdSe core and a ZnS shell, which was coated with anionic (dihydrolipoic acid; DHLA), cationic (cysteamine), zwitterionic

Table 1 Biodistribution and renal filtration as a function of hydrodynamic diameter

Molecule	MW (kDa)	HD (nm)	Urine/blood filterability (%)	Blood half-life (min)	Whole body half-life (h)	Ref.
Inulin	5	3.0	100	9	1.9	18,19
Lysozyme	15	3.4	80	12	1.3	20,21
Myoglobin	17	3.8	75	9	2.0	20,22
ScFv	30	5.3[a]	74	11	1.4	5
Bence-Jones	44	6.1[a]	10	–	3.0	23,24
Fab′	50	6.0	9	28	4.0	4,20
$Sc(Fv)_2$	60	7.0[a]	–	78	5.1	5
Has	67	7.3[a]	0.3	110	16.0	22
$[sc(Fv)_2]_2$	120	9.3[a]	–	170	8.9	5
IgG	152	11.0	<0.1	330	730.0	5,20

[a]Unknown HDs were calculated using the following power law fit to literature values: $HD = A \times MW^B + C \times MW^D$, where $A = -0.000000002614$, $B = 3.326$, $C = 0.9482$ and $D = 0.5001$; $R^2 = 0.999$. HD, hydrodynamic diameter; MW, molecular weight.

[1]Division of Hematology/Oncology, Dept. of Medicine and [3]Dept. of Radiology, Beth Israel Deaconess Medical Center, 330 Brookline Avenue, Room SL-B05, Boston, Massachusetts 02215, USA. [2]Dept. of Chemistry, Massachusetts Institute of Technology, Building 6-221, 77 Massachusetts Avenue, Cambridge, Massachusetts 02139, USA. Correspondence should be addressed to J.V.F. (jfrangio@bidmc.harvard.edu) or M.G.B. (mgb@mit.edu).

Received 13 April; accepted 16 August; published online 23 September 2007; doi:10.1038/nbt1340

(cysteine) or neutral (DHLA-connected polyethylene glycol; DHLA-PEG) small molecules (**Fig. 1a**). The charge of the coating had a profound effect on the adsorption of serum proteins as well as the hydrodynamic diameter; purely anionic or cationic charge was associated with an increase in hydrodynamic diameter >15 nm after incubation with serum (**Fig. 1b**). Although neutral (PEGylated) quantum dots did not bind serum protein, it was not possible to synthesize them with a hydrodynamic diameter $< \approx 10$ nm. Shorter PEG lengths resulted in insoluble quantum dots[3]. Surprisingly, zwitterionic coatings, in this case the amino acid cysteine (Cys), prevented serum protein adsorption while producing the highest solubility and the smallest possible hydrodynamic diameter.

Cys-coated quantum dots (QD-Cys) were characterized by three independent sizing methods (**Fig. 1c**). Transmission electron microscopy was used to measure core/shell diameter, which, as expected, increased with peak fluorescence emission (**Fig. 1d**). Results from dynamic light scattering and gel-filtration chromatography were highly correlated with respect to hydrodynamic diameter after addition of the organic coating (**Fig. 1c** and **Supplementary Fig. 1** online). Using these methods, we created a series of QD-Cys, ranging in final hydrodynamic diameter from 4.36 to 8.65 nm and differing only in peak emission wavelength (515–574 nm; that is, QD515–QD574; **Fig. 1c** and **Supplementary Fig. 2** online), whose hydrodynamic diameter and stability were unchanged after 4 h incubation with 37 °C serum. Electron paramagnetic resonance spectroscopy on QD-Cys samples incubated with spin trapping 5,5-dimethyl-1-pyrroline-N-oxide confirmed that radicals were not produced during photon absorption (see **Supplementary Fig. 3** online).

Initial studies focused on the smallest fluorescent nanoparticle, QD515. After dilution of Cys-coated QD515 in sterile saline and intravenous injection into rat at a dose of 10 pmol/g animal weight, its renal excretion could be visualized directly, as could its transport down the ureters bilaterally and into the bladder (**Fig. 2a** and **Supplementary Video 1** online). Comparison of all quantum dot hydrodynamic diameters (HD) in mice revealed that at 4 h after injection, only QD515 (HD = 4.36 nm), QD534 (HD = 4.99 nm) and QD554 (HD = 5.52 nm) could be found excreted into the bladder (**Fig. 2b**), with fluorescent intensity decreasing as hydrodynamic diameter increased. The larger quantum dots, including DHLA-, cysteamine- and DHLA-PEG–coated ones, were never found in the bladder but, instead, were trapped in the liver, lung and spleen in large amounts (data not shown).

Because *in vivo* fluorescence imaging provides only a qualitative, semiquantitative measurement of quantum dot behavior *in vivo*, we developed a technique to label the QD-Cys surface covalently with a chelated form of the gamma ray–emitting isotope ^{99m}Tc. Despite noncovalent interaction of cysteine with the quantum dot surface, no aggregates were detectable by high-performance liquid chromatography (HPLC) analysis, and the amount of unbound isotope was <10%

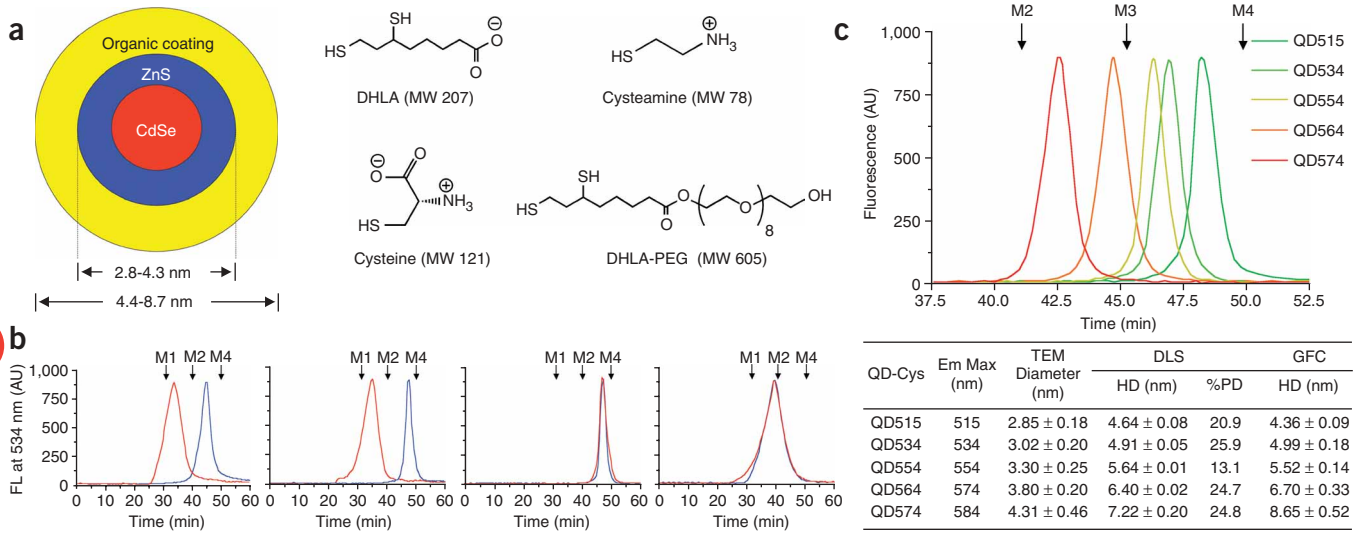

QD-Cys	Em Max (nm)	TEM Diameter (nm)	DLS HD (nm)	DLS %PD	GFC HD (nm)
QD515	515	2.85 ± 0.18	4.64 ± 0.08	20.9	4.36 ± 0.09
QD534	534	3.02 ± 0.20	4.91 ± 0.05	25.9	4.99 ± 0.18
QD554	554	3.30 ± 0.25	5.64 ± 0.01	13.1	5.52 ± 0.14
QD564	574	3.80 ± 0.20	6.40 ± 0.02	24.7	6.70 ± 0.33
QD574	584	4.31 ± 0.46	7.22 ± 0.20	24.8	8.65 ± 0.52

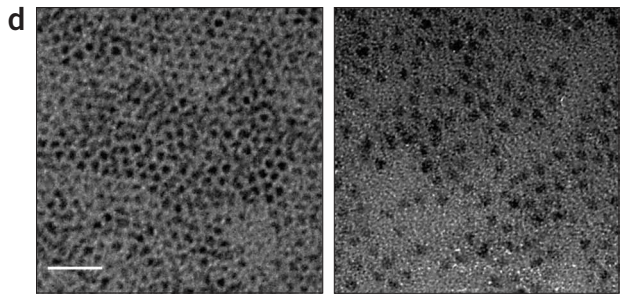

Figure 1 Design of fluorescent quantum dots, measurement of hydrodynamic diameter and interaction of the organic coating with serum proteins. (**a**) Chemical compositions of CdSe/ZnS quantum dots with DHLA (anionic), cysteamine (cationic), cysteine (zwitterionic) and DHLA-PEG (neutral) coatings. (**b**) GFC (mobile phase, PBS, pH 7.4) of quantum dots (CdSe/ZnS core/shell, diameter 3.02 nm) with organic coatings shown in **a**, after treatment with PBS, pH 7.4 (blue line) or FBS (red line). $\lambda_{exc} = 414$ nm; $\lambda_{em} = 534$ nm. Molecular weight markers M1 (thyroglobulin; 669 kDa, 18.0 nm HD), M2 (γ-globulin; 158 kDa, 11.9 nm HD), M3 (ovalbumin; 44 kDa, 6.13 nm HD) and M4 (myoglobin; 17 kDa, 3.83 nm HD) are shown by arrows. (**c**) The emission wavelength of cysteine-coated quantum dots (QD-Cys) increased with the size of core/shell, measured by transmission electron microscopy (TEM), dynamic light scattering (DLS), and GFC. TEM size data for each sample were determined from the average of ≥150 measurements. DLS and GFC measurements (mean ± s.d.) were from $N = 3$ independent experiments. %PD = poly-dispersity. (**d**) TEM pictures of QD515 (left, core/shell 2.85 nm) and QD574 (right, core/shell 4.31 nm). Scale bar, 20 nm. (**e**) GFC (mobile phase, PBS, pH 7.4) of QD-Cys of various hydrodynamic diameters. $\lambda_{exc} = 414$ nm, $\lambda_{em} = 554$ nm. Molecular weight markers (arrows) are as described in **a**.

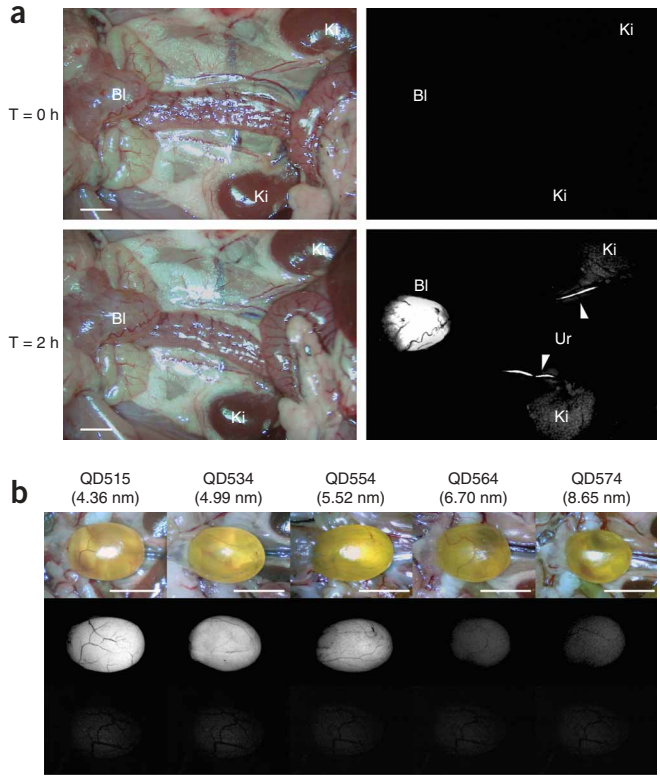

Figure 2 *In vivo* fluorescence imaging of intravenously injected QD-Cys. (**a**) Kidneys (Ki), ureters (Ur; arrowheads) and bladder (Bl) either $T = 0$ (top) or $T = 2$ h (bottom) after intravenous injection of QD515 into the rat. Left, color video; right, fluorescence. Scale bar, 1 cm. (**b**) Surgically exposed CD-1 mouse bladders after intravenous injection of QD515, QD534, QD554, QD564 or QD574 of defined hydrodynamic diameter. Shown are color video (top) and fluorescence images (bottom) for uninjected control bladder and 4 h after injection (middle) for each quantum dot. A 525 ± 25-nm emission filter was used for QD515 and QD534. A 560 ± 20-nm filter was used for QD554, QD564 and QD574. The exposure time (200 ms) and normalizations were the same for all fluorescence images. Scale bar, 1 cm.

in each preparation. Intravenous injection of ^{99m}Tc-labeled quantum dots revealed that changes in final hydrodynamic diameter resulted in dramatic changes in blood half-life (**Fig. 3a**). Indeed, based on the β-phase terminal half-life ($t_{1/2\beta}$), the blood half-life of quantum dots ranged from 48 min to 20 h as the hydrodynamic diameter increased from 4.36 to 8.65 nm (**Fig. 3b**).

Using ^{99m}Tc-labeled quantum dots, we followed distribution and clearance in all organs, and from the body itself, over time. Notably, radiolabeled quantum dots remained intact, even after excretion into urine (see **Supplementary Fig. 4** online), suggesting that gamma ray emission could be used as a reliable surrogate for quantum dot distribution. Four hours after intravenous injection of QD515 (HD = 4.36 nm), the dominant signal was in the bladder. The only appreciable distribution in other organs was in the liver (4.5 ± 1.0% injected dose; ID) and kidney (2.6 ± 0.4%ID), with the latter likely representing quantum dots in the process of being excreted (**Fig. 3c**). In contrast, QD574 (HD = 8.65 nm) exhibited high uptake in liver (26.5 ± 3.9%ID), lung (9.1 ± 4.0%ID) and spleen (6.3 ± 2.4%ID) and a proportionally lower signal in bladder (**Fig. 3d**).

By measuring the radioactivity of both excreted and pre-excreted urine, as well as of the entire remaining carcass excluding bladder and urethra, we defined the relationship between hydrodynamic diameter, renal clearance and total body retention. This relationship was sigmoidal, with the 50% point for total body clearance of quantum dots at 4 h being HD ≈ 5.5 nm (**Fig. 3e**).

Inorganic, metal-containing nanoparticles require a solubilizing organic coating for biological (that is, aqueous) compatibility. In the case of quantum dots, this coating is also a requirement for maintaining photoluminescence efficiency. Unfortunately, organic coatings often result in a significant increase of the final hydrodynamic diameter. Our results suggest that both the molecular weight and charge of the solubilizing ligand contribute to final hydrodynamic diameter *in vivo* and that pure charge (anionic or cationic) is associated with unexpected serum protein adsorption. This adsorption did not appear to affect solubility but increased hydrodynamic diameter by almost 15 nm.

Nanoparticle hydrodynamic diameter is a critical design parameter in the development of potential diagnostic and therapeutic agents. The mammalian vasculature has an average pore size of ~5 nm. Below this value, there is relatively fast equilibrium between agents injected intravenously and the extracellular space, but, above this value, transport across the endothelium is remarkably slow. For example, human IgG (HD ≈ 10 nm) requires ~24 h to equilibrate between the vascular and extracellular spaces after intravenous injection[4,5]. To a first approximation, glomerular filtration in the kidney is controlled by similar effective pore sizes, and renal excretion is a strong function of hydrodynamic diameter (**Table 1**). For nanoparticles that do not biodegrade *in vivo* into biologically benign components, the only other major route of excretion from the human body is through the liver, into bile and into feces. The problems with liver excretion for nanoparticles are threefold. First, the liver is designed specifically to capture and eliminate nanoparticles (e.g., viruses) > ~10–20 nm in hydrodynamic diameter. Hence, special coatings such as PEG are required just to prevent first-pass extraction from the reticuloendothelial system (liver, spleen and bone marrow), but these coatings necessarily increase hydrodynamic diameter. Dense PEGylation might increase blood half-life, but it also precludes elimination from the body. Second, excretion of intact nanoparticles into bile is an extremely slow and inefficient process. Third, long-term retention in the reticuloendothelial system leads to a large area under the exposure -time curve and increases the likelihood of toxicity. At the very least, our data suggest that analysis of bodily fluids, including urine and bile, should be part of human risk assessment after environmental exposure to nanoparticles and can help estimate total retained dose if the exposure dose is known.

The importance of total body clearance of nanometer-sized objects is not a trivial one. Consider, for example, what would occur if retention affected other medical tests. Radiological tests are particularly susceptible. Metals with high atomic numbers deposited in organs would interfere with X-ray imaging (that is, plain films, fluoroscopy and CT) because of changes in linear attenuation coefficient, magnetic resonance imaging because of proton-free voids, ultrasound because of increased echogenicity, and possibly even single-photon emission computed tomography and positron emission tomography (PET) because of photon attenuation (both) and/or effects on positronium production (PET). Renally cleared nanoparticles, even metal-containing ones, would minimize or eliminate these problems.

Several caveats, though, must be considered. First, the absolute value for the renal filtration threshold (HD = 5.5 nm in this study) depends on the calibration curves of the sizing techniques. Because

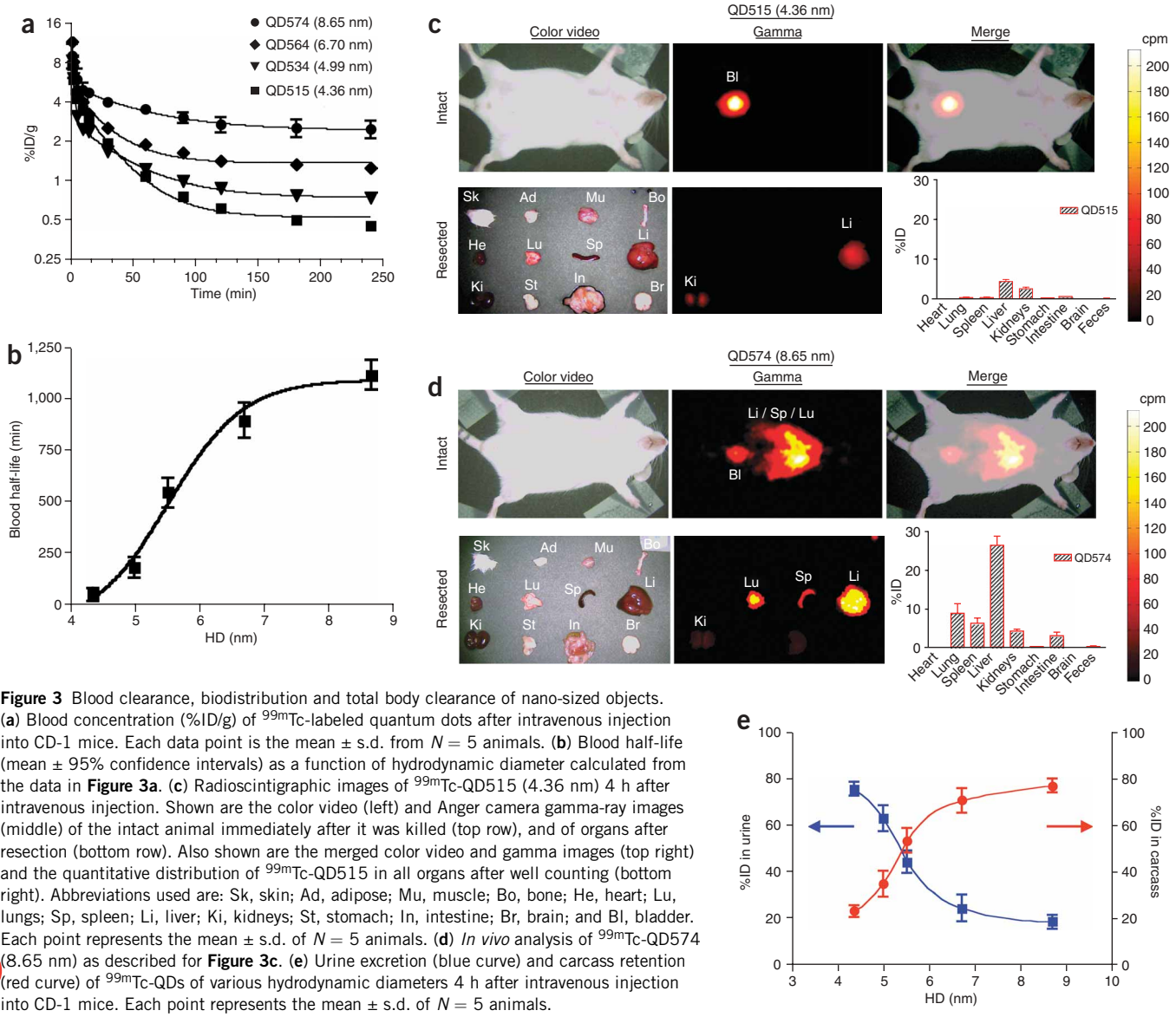

Figure 3 Blood clearance, biodistribution and total body clearance of nano-sized objects. (**a**) Blood concentration (%ID/g) of ^{99m}Tc-labeled quantum dots after intravenous injection into CD-1 mice. Each data point is the mean ± s.d. from $N = 5$ animals. (**b**) Blood half-life (mean ± 95% confidence intervals) as a function of hydrodynamic diameter calculated from the data in **Figure 3a**. (**c**) Radioscintigraphic images of ^{99m}Tc-QD515 (4.36 nm) 4 h after intravenous injection. Shown are the color video (left) and Anger camera gamma-ray images (middle) of the intact animal immediately after it was killed (top row), and of organs after resection (bottom row). Also shown are the merged color video and gamma images (top right) and the quantitative distribution of ^{99m}Tc-QD515 in all organs after well counting (bottom right). Abbreviations used are: Sk, skin; Ad, adipose; Mu, muscle; Bo, bone; He, heart; Lu, lungs; Sp, spleen; Li, liver; Ki, kidneys; St, stomach; In, intestine; Br, brain; and Bl, bladder. Each point represents the mean ± s.d. of $N = 5$ animals. (**d**) *In vivo* analysis of ^{99m}Tc-QD574 (8.65 nm) as described for **Figure 3c**. (**e**) Urine excretion (blue curve) and carcass retention (red curve) of ^{99m}Tc-QDs of various hydrodynamic diameters 4 h after intravenous injection into CD-1 mice. Each point represents the mean ± s.d. of $N = 5$ animals.

the reported hydrodynamic diameters of the molecules used for calibration vary in the literature by as much as 10%, so too must our confidence in the 5.5-nm cutoff. For this reason, it will be important to test each nanometer-sized object independently *in vivo*, and not rely solely on *in vitro* predictions. Second, our study has not addressed the effect of nanoparticle shape on renal filtration. For example, quantum rods[6] and other nonspherical nanoparticles will need separate *in vivo* analyses. If eventual results correlate with those from long rigid proteins, it is likely that the long axis of the particle will dominate its *in vivo* behavior. Finally, our study suggests that molecularly targeting quantum dots and other nanoparticles requires careful attention to hydrodynamic diameter. Indeed, our results suggest that only extremely small targeting molecules will be of use for *in vivo* targeting if renal excretion is to be maintained. Fortunately, the increased affinity associated with multimerization of such ligands on the quantum dot surface[7] may permit a small number of targeting ligands to be used relative to coating ligands.

Thus far, few nanometer-sized objects are being actively translated to the clinic. Our study suggests that to satisfy both patient safety and regulatory review, nanoparticle biodistribution and clearance must be carefully considered. We propose three criteria for distinguishing a nanoparticle that has potential clinical utility: (i) a final HD $\leq$ 5.5 nm to permit complete elimination from the body and/or (ii) a formulation with completely nontoxic components and/or (iii) biodegradability to clearable components. We suggest that metal-containing nanoparticles that do not satisfy these criteria will have limited clinical utility.

METHODS

Synthesis of CdSe/ZnS core/shells. CdSe/ZnS core/shell nanocrystals were synthesized using the following methods: QD515 (ref. 8), QD534 (refs. 9,10), QD554 (refs. 9,10), QD564 (refs. 9,10) and QD574 (refs. 9,10). See **Supplementary Methods** online for detailed experimental methods.

DHLA and DHLA-PEG organic coatings. Dihydrolipoic acid (DHLA) and DHLA conjugated to a polyethylene glycol spacer ($n = 8$, DHLA-PEG) was prepared using procedures from the literature[3,11]. Ligand exchange was performed according to reported procedures[3,11], with modifications. Briefly, an aliquot of quantum dot growth solution (0.2 ml) was precipitated with the

addition of acetone followed by centrifugation at 3,500*g* for 4 min. The supernatant was discarded, and 50 µl of neat DHLA or DHLA-PEG along with 50 µl of methanol was added to the pellet. The mixture was stirred at 60 °C for 2 h and precipitated with the addition of ethanol, chloroform and hexane followed by centrifugation at 3,500*g* for 4 min. The supernatant was discarded and the quantum dot sample was redispersed in PBS (pH 7.4) for analysis.

Cysteine and cysteamine organic coatings. Ligand exchange with cysteine and cysteamine was carried out using a biphasic exchange method, in which quantum dots size-selectively precipitated twice using acetone were redispersed in $CHCl_3$ to which a solution of cysteine (40 mg/ml) or cysteamine (50 mg/ml) in PBS (1 ml) was added. This biphasic mixture was stirred vigorously for 2–6 h until the organic layer became colorless. The $CHCl_3$ phase was removed by pipette and residual organic solvent removed under reduced pressure. The quantum dots were precipitated twice with the addition of ethanol and redispersed in PBS (pH 7.4) for analysis. The cysteine-coated quantum dots (QD-Cys) were stabilized by adding dithiothreitol (DTT, 1 mM) to prevent the dimerization of cysteine. QD-Cys formulations treated in this fashion are stable for up to 1 week in PBS, pH 7.4 storage buffer under ambient conditions and exhibit quantum yields of 10–15% (see **Supplementary Methods** and **Supplementary Fig. 5** online). Before conjugation, any free ligands were removed by three cycles of dilution/concentration through Vivaspin 6 (MWCO 10,000) spin concentrators (Vivascience).

TEM sizing of quantum dot core/shell. The size of CdSe/ZnS core/shell structures was measured using a JEOL 200CX TEM operating at 200 kV. One drop of a dilute sample of quantum dots in hexane was placed onto a Formvar-coated copper grid, allowed to settle for 20 s and wicked away using an absorbent tissue. Size analysis was performed on captured digital images using ImageJ V. 1.34s.

Hydrodynamic diameter measurements by dynamic light scattering. Light scattering analysis was performed on a DynaPro Dynamic Light Scattering system (Qyatt). The concentration of stock quantum dots was 2–3 µM, and all quantum dots were filtered through a 0.02-µm filter before analysis. Typical count rates were 100–300 kHz. Each autocorrelation function (ACF) was acquired for 10 s and averaged for 10 min per measurement. A software filter was used to discard all ACF fits with sum of squares errors >15. The resulting ACF was fitted using the Dynamics V6 software employing a nonnegative least-squares fitting algorithm. Hydrodynamic size data were obtained from a mass weighted size distribution analysis and reported as the mean of triplicate measurements ± s.d.

Gel-filtration chromatography (GFC). Details of the custom GFC system, which permits on-line, full-spectrum analysis of quantum dot absorbance and fluorescence, have been published previously[12]. GFC was performed on a Superose-6 10/300 GL column (Amersham Biosciences) using PBS, pH 7.4 supplemented with 1 mM cysteine as mobile phase. Flow rate was 0.4 ml/min. Calibration (see **Supplementary Methods**) of hydrodynamic diameter was performed by injecting 50 µl of protein standards (cat. 151-1901, Bio-Rad) containing thyroglobulin (669 kDa, 18.0 nm HD), γ-globulin (158 kDa, 11.9 nm HD), ovalbumin (44 kDa, 6.13 nm HD), myoglobin (17 kDa, 3.83 nm HD) and vitamin B_{12} (1.35 kDa, 1.48 nm HD). All hydrodynamic diameter measurements were performed with three independent experiments. For measurement of the effects of serum protein adsorption, 1 µM quantum dots were incubated in PBS or 100% FBS (FBS) for 4 h at 37 °C before loading of 100 µl onto the GFC column.

^{99m}Tc-labeling of quantum dots. Preparation of high-specific-activity N-hydroxysuccinimide (NHS) ester of ^{99m}Tc-MAS_3, in neat aprotic solvent, has been described previously[13]. See **Supplementary Methods** for detailed experimental methods and **Supplementary Figure 6** online. ^{99m}Tc-quantum dot conjugation was performed by the addition of 80 µl of ^{99m}Tc-MAS_3-NHS (2 mCi) in DMSO to 1 ml of quantum dots (1 µM) in PBS, pH 7.8. After stirring for 1 h, the radiolabeled conjugates were purified by washing five times in Vivaspin concentrators (MWCO 10,000) with pH 7.4 PBS and analyzed by RP-HPLC on a 8 × 300 mm, 200 Å Diol (YMC) size-exclusion column using PBS, pH 7.4 supplemented with 1 mM cysteine as mobile phase. Details of the RP-HPLC system have been described previously[14].

Animal models. Animals were housed in an Association for the Assessment and Accreditation of Laboratory Animal Care–certified facility staffed by full-time veterinarians and were studied under the supervision of an approved institutional protocol. Sprague-Dawley (SD) male rats, weighing 300–350 g, were purchased from Taconic Farms and 30 g CD-1 male mice were from Charles Laboratories. All animals acclimated to the animal facility for at least 48 h before experimentation. For surgery, rats and mice were anesthetized with 65 mg/kg intraperitoneal pentobarbital. Quantum dots in saline ($N = 5$ mice each) were administered intravenously at a dose of 10 pmol/g of animal weight (1 ml of a 3-µM stock solution for rats and 100 µl of a 3-µM stock solution for mice). After each study, animals were killed by intraperitoneal injection of 200 mg/kg pentobarbital, a method consistent with the recommendations of the Panel on Euthanasia of the American Veterinary Medical Association.

Intraoperative fluorescence imaging. An intraoperative fluorescence imaging system optimized for animal surgery has been described in detail previously[15–17]. For fluorescence excitation, three 100-mW L470-66-60 LEDs (Marubeni Epitex) fitted with 470 ± 20 nm excitation filters in custom holders were used. Emission filters were 525 ± 25 nm or 560 ± 20 nm, depending on quantum dot. The exposure time (200 ms) and normalizations were the same for all fluorescence images. Color video was collected on a separate optical channel using computer-controlled camera acquisition via custom LabVIEW (National Instruments) software.

Quantum dot biodistribution and clearance. 100 µl of 3 µM ^{99m}Tc-QDs (~250 µCi) were administered intravenously to $N = 5$ CD-1 mice per quantum dot. Mice were housed in special cages to allow for the collection of urine and feces. Measurement of blood clearance was performed by intermittent sampling of the tail vein. Mice were killed 4 h after injection. To measure total urinary excretion, we ligated the ureters and urethra with silk sutures, and removed the bladder *en masse* and combined it with excreted urine, before measurement of radioactivity in a dose calibrator. The remaining carcass was also measured in a dose calibrator, then the skin, adipose, muscle, bone, heart, lungs, spleen, liver, kidneys, stomach, intestine, brain and feces were resected, washed twice in PBS, pH 7.4, weighed, and their radioactivity measured on a Wallac Wizard (model 1470, Perkin Elmer) 10-detector gamma counter. Curve fitting was performed using Prism version 4.0a (GraphPad) software. Gamma radioscintigraphy was performed with a Research Digital Camera (Isocam Technologies) equipped with a 1/2" NaI crystal, 86 photo-multiplier tubes and high-resolution (1 mm) low-energy lead collimator.

Note: Supplementary information is available on the Nature Biotechnology website.

ACKNOWLEDGMENTS

The Biophysical Instrumentation Facility for the Study of Complex Macromolecular Systems (NSF-0070319 and NIH GM68762) is gratefully acknowledged. This work was supported in part by the US National Science Foundation–Materials Research Science and Engineering Center Program under grant DMR-9808941 (M.G.B.), National Institutes of Health (NIH) grant no. R21/R33 EB-000673 (J.V.F. and M.G.B.), and a fellowship from the Charles A. King Trust, Bank of America, Co-Trustee (H.S.C.). M.G.B. also acknowledges support from the NIH-funded Massachusetts Institute of Technology–Harvard NanoMedical Consortium (1U54-CA119349, a Center of Cancer Nanotechnology Excellence). We thank Barbara L. Clough for medical editing and Grisel Vazquez for administrative assistance.

Published online at http://www.nature.com/naturebiotechnology/
Reprints and permissions information is available online at http://npg.nature.com/reprintsandpermissions

1. Hardman, R. A toxicologic review of quantum dots: toxicity depends on physico-chemical and environmental factors. *Environ. Health Perspect.* **114**, 165–172 (2006).
2. Ballou, B. *et al.* Sentinel lymph node imaging using quantum dots in mouse tumor models. *Bioconjug. Chem.* **18**, 389–396 (2007).
3. Uyeda, H.T., Medintz, I.L., Jaiswal, J.K., Simon, S.M. & Mattoussi, H. Synthesis of compact multidentate ligands to prepare stable hydrophilic quantum dot fluorophores. *J. Am. Chem. Soc.* **127**, 3870–3878 (2005).

4. Chapman, A.P. *et al.* Therapeutic antibody fragments with prolonged *in vivo* half-lives. *Nat. Biotechnol.* **17**, 780–783 (1999).
5. Goel, A. *et al.* Genetically engineered tetravalent single-chain Fv of the pancarcinoma monoclonal antibody CC49: improved biodistribution and potential for therapeutic application. *Cancer Res.* **60**, 6964–6971 (2000).
6. Fu, A. *et al.* Semiconductor quantum rods as single molecule fluorescent biological labels. *Nano Lett.* **7**, 179–182 (2007).
7. Mammen, M., Choi, S.K. & Whitesides, G.M. Polyvalent interactions in biological systems: implications for design and use of multivalent ligands and inhibitors. *Angew. Chem. Int. Ed. Engl.* **37**, 2754–2794 (1998).
8. Peng, Z.A. & Peng, X. Formation of high-quality CdTe, CdSe, and CdS nanocrystals using CdO as precursor. *J. Am. Chem. Soc.* **123**, 183–184 (2001).
9. Dabbousi, B.O. *et al.* (CdSe)ZnS core-shell quantum dots: synthesis and characterization of a size series of highly luminescent nanocrystallites. *J. Phys. Chem. B* **101**, 9463–9475 (1997).
10. Fisher, B.R., Eisler, H.-J., Stott, N.E. & Bawendi, M.G. Emission intensity dependence and single-exponential behavior in single colloidal quantum dot fluorescence lifetimes. *J. Phys. Chem. B* **108**, 143–148 (2004).
11. Mattoussi, H. *et al.* Self-assembly of CdSe-ZnS quantum dot bioconjugates using an engineered recombinant protein. *J. Am. Chem. Soc.* **122**, 12142–12150 (2000).
12. Frangioni, J.V., Kim, S.W., Ohnishi, S., Kim, S. & Bawendi, M.G. Sentinel lymph node mapping with type-II quantum dots. *Methods Mol. Biol.* **374**, 147–160 (2007).
13. Misra, P., Humblet, V., Pannier, N., Maison, W. & Frangioni, J.V. Production of multimeric prostate-specific membrane antigen small molecule radiotracers using a solid-phase 99mTc pre-loading strategy. *J. Nucl. Med.* **48**, 1379–1389 (2007).
14. Humblet, V., Misra, P. & Frangioni, J.V. An HPLC/mass spectrometry platform for the development of multimodality contrast agents and targeted therapeutics: prostate-specific membrane antigen small molecule derivatives. *Contrast Media Mol. Imaging* **1**, 196–211 (2006).
15. Kim, S. *et al.* Near-infrared fluorescent type II quantum dots for sentinel lymph node mapping. *Nat. Biotechnol.* **22**, 93–97 (2004).
16. De Grand, A.M. & Frangioni, J.V. An operational near-infrared fluorescence imaging system prototype for large animal surgery. *Technol. Cancer Res. Treat.* **2**, 553–562 (2003).
17. Nakayama, A., del Monte, F., Hajjar, R.J. & Frangioni, J.V. Functional near-infrared fluorescence imaging for cardiac surgery and targeted gene therapy. *Mol. Imaging* **1**, 365–377 (2002).
18. Pappenheimer, J.R., Renkin, E.M. & Borrero, L.M. Filtration, diffusion and molecular sieving through peripheral capillary membranes; a contribution to the pore theory of capillary permeability. *Am. J. Physiol.* **167**, 13–46 (1951).
19. Prescott, L.F., McAuslane, J.A. & Freestone, S. The concentration-dependent disposition and kinetics of inulin. *Eur. J. Clin. Pharmacol.* **40**, 619–624 (1991).
20. Olmsted, S.S. *et al.* Diffusion of macromolecules and virus-like particles in human cervical mucus. *Biophys. J.* **81**, 1930–1937 (2001).
21. Hansen, N.E., Karle, H. & Andersen, V. Lysozyme turnover in the rat. *J. Clin. Invest.* **50**, 1473–1477 (1971).
22. Lund, U. *et al.* Glomerular filtration rate dependence of sieving of albumin and some neutral proteins in rat kidneys. *Am. J. Physiol. Renal Physiol.* **284**, F1226–F1234 (2003).
23. Solomon, A., Waldmann, T.A., Fahey, J.L. & McFarlane, A.S. Metabolism of Bence Jones Proteins. *J. Clin. Invest.* **43**, 103–117 (1964).
24. Bradwell, A.R., Carr-Smith, H.D., Mead, G.P., Harvey, T.C. & Drayson, M.T. Serum test for assessment of patients with Bence Jones myeloma. *Lancet* **361**, 489–491 (2003).